Numerical Investigation of the Effect of Inflow Distortions on Transonic Axial Compressor Stages

Andreas Lesser, Roberto Ciorciari, Sebastian Barthmes and Reinhard Niehuis
Institut für Strahlantriebe
Universität der Bundeswehr München Werner-Heisenberg-Weg 39 85577 Neubiberg

Abstract

This paper refers to numerical and experimental research activities on the effect of inhomogeneous inflow to transonic axial compressors. The presence of inhomogeneous inflow (inlet distortions) not only affects the performance of the compressor itself but also of the entire propulsion system. Typically, this means loss in the stall margin as well as loss in efficiency. In the worst case, this may lead to an unstable operation (surge) and complete loss of thrust. As a very important safety issue, the effect of inlet distortions on stability and performance has been a crucial field of research during/for the last decades. Due to the outcome of increasingly powerful CFD tools and of high performance computers better predictions capabilities become available. However the CFD methods need to be further developed and validated in order to allow a reliable performance prediction. In the context of future highly efficient airplane concepts, the problem of a distorted inflow came into focus again as some of these new designs consider highly integrated jet engines. These jet engines require complex intakes, or other engine installations which considerably deteriorate the flow before entering the compressor. New compressor designs are necessary to better cope with inlet distortions. In this study the effects of inflow distortions on the stability behavior as well as on the efficiency have been investigated numerically in detail. Two transonic compressor test cases have been simulated with the flow solver TRACE developed by the German research center for aeronautics and space (DLR). The first test case is a transonic compressor stage, which was experimentally investigated by the DLR. The other compressor stage has been examined at the TU Darmstadt. The two compressors have been tested with different kinds of total pressure distortions. While the DLR compressor was run with a steady, radially constant distortion in a 120° sector, the TU Darmstadt compressor was exposed to an unsteady distortion featuring variations in radial and circumferential direction. The numerical results have been carefully validated with available experimental data and evaluated considering the influence of the different distortions on the overall performance of the compressor. Additionally, detailed flow analyses have been performed in order to identify the relevant flow phenomena which are responsible for the particular compressor performance under the presence of inlet distortions.

I. Introduction

THIS paper refers to numerical investigations of compressor stages with inhomogeneous inflow conditions. Engines working with compressors with inhomogeneous inflow conditions get in the focus of research for several reasons the last years. Rising fan bypass ratios leading to higher fan diameter and lower inlet - fan diameter ratios, therefore the inlets ability to homogenize the inflow is lower. Another example for the importance of engines working with distorted inflow conditions, are boundary layer ingesting engines, for future airframe concepts. These engines are impinged permanently with the fuselages laminar boundary layer. For all these different scenarios the engine is supposed to work stable as well as efficiently. Actual research can be separated into two parts. The first part focuses on inlet aerodynamics. Distortions that arise in the inlet are investigated with emphasis of their

generation and development in front of the compressor entry plane. The origin of these distortions may be crosswind [1], [2], high angle of attack [3], ground vortices sucked into the engine [4] or highly transient maneuvers in flight [5]. A notable similarity between these studies is that in each compressor aerodynamic is not the focal point. On the other hand there is still a lot of research on compressor aerodynamics considering a distorted inflow. For the experiments the distortions have been generated using plates or screens, which can be steady [6] or transient while producing a total pressure and inflow angle distortions. However, a transient distortion can be steady from the compressors point of view. The distortion investigated by [7] is transient as the time scales are so long that it can be considered as steady compared to the much shorter time scales of the compressor passing frequency. For numerical investigations the distortions are typically modeled as inlet boundary conditions [8], [9] or with actuator disk approaches. One objective of the research work published in this paper was to generate an inlet distortion with a well proven approach like modifying an inlet boundary condition. Additionally the source of distortion in the computational domain has been included, to study also the interaction between the origin of the distortion and the compressor.

In order to achieve this objective two compressor test cases have been selected. The first one is a transonic compressor stage with a total pressure and inflow angle distortion investigated by the DLR in Cologne [10]. The second compressor was a new test case which was both experimentally and numerically designed to be able to be computed in one computational domain. For the investigations the transonic compressor rig at the TU Darmstadt has been chosen. The numerical investigations will be presented below.

II. TEST CASES AND NUMERICAL PROCEDURE

1. DLR TEST CASE AND TEST ROTOR

The first examined compressor in this study is a transonic high-pressure compressor, operated at the DLR AT (Dunker [11], [12] and Lecht [10]). The experimental setup can be seen in Figure 1. The compressor stage has been designed for a radial constant work input and axial inlet and outlet flow. The global design parameters at peak efficiency conditions are a spool speed of 20260 RPM, a total pressure ratio of 1.51 and an equivalent mass flow of 17.3 kg/s under international standard atmosphere (ISA) conditions (T_{to}= 288 K, P_{to} = 101325 Pa). The rotor is designed with Double-circular-arc-blades (DCA) for the subsonic part near hub and with multiple-circular-arc-blades (MCA) for the supersonic part near tip where the maximum relative inflow Mach number 1.4 is reached. Overall, 28 blades with an average chord length of 50 mm were used. The stator consists in 72 vanes with NACA-65 profiles.

For this configuration, detailed measurements of temperature, pressure, and flow direction exist only with disturbed inflow conditions. For all measurements data on turbulent intensity and turbulent length scale are not available. Anyway, this compressor stage has been chosen for CFD studies since this test case was the only publically available one since many years before the compressor stage with inlet distortions at TU Darmstadt became available within the DFG research group FOR 1066.

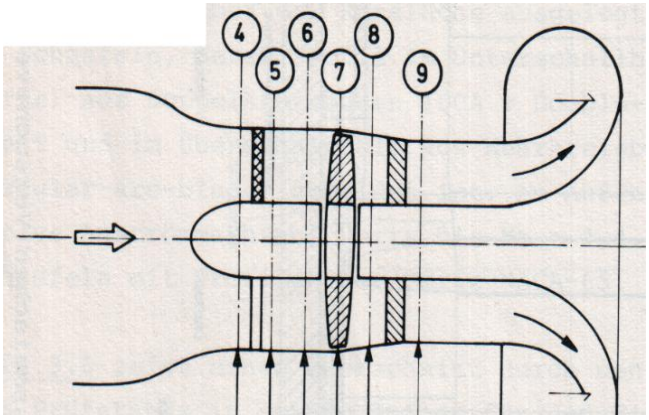

Figure 1 TRANSONIC COMPRESSOR STAGE TEST RIG [10]

A summary of the main design parameters of the compressor will be given on Table **1**. The total pressure inlet distortion was generated upstream of the compressor stage by a non-rotating wake generator with steel bars. The circumferential extent of the investigated distortions was 60 and 120 degrees. As most of the published experimental data refers to the 120° distortion the numerical investigations were carried out with 120° distortion.

2. TUD Test Case and Test Rotor

The second test case investigated is the transonic compressor rig at the Technische Universität Darmstadt (TUD). In this open circuit facility ambient air is sucked into the compressor. To guarantee a homogeneous inflow the sucked air passes a settling chamber before entering the compressor intake. A schematic sketch is shown in Figure **2** on the left hand side. The compressor was used with a/the Rotor-1/Stator-1 configuration. The rotor and stator consist of 16 blades or 29 vanes. General design features are listed in Table **1** on the right hand side. More information about this compressor configuration is provided in [13], [14]. To generate an unsteady, radial and circumferential distortion a distortion generator was designed which provide these features. More details of the design will be discussed later on and are available in [15].
The compressor casing was modified to allow unsteady total pressure measurements in various axial planes. Additionally, the steady total pressure and total temperature distributions behind the stator was measured. The detailed experimental setup and first experimental results are published in [16].

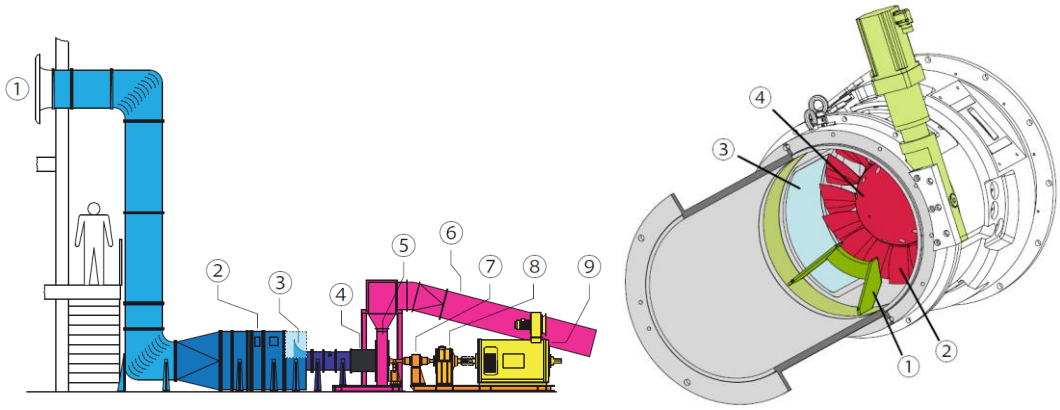

Figure 2: TUD TRANSONIC COMPRESSOR FACILITY (LEFT) AND COMPRESSOR STAGE WITH DISTORTION GENERATOR (RIGHT)[16]

Table 1: DESIGN PARAMETERS AT DESIGN POINT OF THE DLR TEST CASE (LEFT) AND THE TU DARMSTADT TEST CASE (RIGHT)

Corrected Mass Flow Rate	$17.3\,\frac{kg}{s}$	$16\,\frac{kg}{s}$
Total Pressure Rate	1.5	1.5
Corrected Tip Speed at 100% shaft speed	$424\,\frac{m}{s}$	$398\,\frac{m}{s}$
Shaft Speed	20260 rpm	20000 rpm
Tip Clearance gap	0.3 mm	1.6 mm
Number of Blades	28	16
Number of Vanes	72	29

3. Numerical Procedure

Solver

The numerical investigations presented in this paper have been carried out using the flow solver TRACE. The flow solver, developed by DLR AT in collaboration with MTU Aero Engines, is using the unsteady Reynolds averaged Navier-Stokes equations with a finite volume approach and is optimized for the computation of internal flows in turbomachines. The convective fluxes are discretized using the TVD upwind scheme by Roe [17] that is combined with a MUSCL extrapolation scheme to reach second order spatial accuracy. All diffusive fluxes are discretized

using a second order central differencing scheme. For steady state calculations which are presented in this study a time marching technique with an implicit predictor corrector scheme has been used. The dual time stepping approach used for the unsteady calculations utilizes an implicit Euler scheme within the pseudo-time level while a second order accurate predictor-corrector scheme is used for the physical time integration. The resulting linear system of equations is iteratively solved by a symmetric Gauss-Seidel relaxation scheme. Furthermore non-reflecting inflow and outflow boundary conditions are implemented. Turbulent flow is taken into account by using the Wilcox [18] k-ω turbulence model which is extended by a time scale bound by Durbin and Peterson-Reif [19] in order to avoid an unrealistic production of turbulence near stagnation points. For more detailed information about TRACE refer to Kožulović et al.[20], [21], Yang et al. [22], [23], Nürnberger [24], Eulitz [25].

Simulation Setup

All grids were created by the meshing tool G3DHEXA, also has been developed by the DLR-AT. In compressors with a distorted inflow the following flow phenomena are characterized by different turbulent length scales. All relevant non-modeled flow phenomena, i.e. in case of URANS simulations all non-turbulent flow features, have to be resolved. Here the grid has to guarantee that relevant flow phenomena are resolved and no relevant grid sensitivity is present. In order to maintain these constraints highly resolving structured grids were chosen. The grid blocks for the blades and vanes are featuring an OCH topology and a special H-block was chosen in the tip gap. These parameters are producing, for the DLR test case, a total number of 50 million cells. The steady inflow distortion was modeled by a Riemann boundary condition, which was modified to read in the inlet flow field, which was given by the measured flow field. In a common turbomachinery approach for hub and tip walls wall function were used and low Reynolds treatment for blades and vanes.
In the TUD test case the source of the distortion, the distortion generator, was designed to be able to be numerically taken into account, too. The joint simulation of the origin of the distortion and the compressor allows the investigation of the interaction between distortion and compressor. As the designed distortion body and especially its mounting part are difficult to mesh with structured grids a hybrid mesh approach has been chosen. The intake of the compressor up to about one axial chord length upstream of the leading edge has been meshed with an unstructured grid. Subsequently, the rotor and stator are meshed with structured grids. The structured grid is quite similar to the grid used for the DLR test case, but the tip gap is refined. In total this grid has nearly 56 million cells. The hybrid unstructured mesh, here with a prismatic wall layer to resolve the boundary layers at viscid walls and tetra elements to fill, represents the intake section and the distortion body and is built up by 60 million elements. Hence, the whole domain consists of 120 million elements. The flow simulations were performed at the Leibniz Supercomputing Centre in Munich.

III. RESULTS

1. DLR TEST CASE

The validation and the summarized results of the simulation of the DLR test case will be presented in the following.
In Figure **3** the used inlet boundary total pressure and inflow angle distribution is shown. A wake generator formed by non-rotating steel bars causes a 120° total pressure distortion. Also an inflow angle variation is generated due to flow redistribution, caused by static pressure gradients due to the total pressure distortion. The variation of the inflow angle extent the 120° sector of the total pressure variation, as can be seen in Figure **3** on the right hand side. Only measurement data for mid-span was available, hence the distortion was assumed to be radial constant.

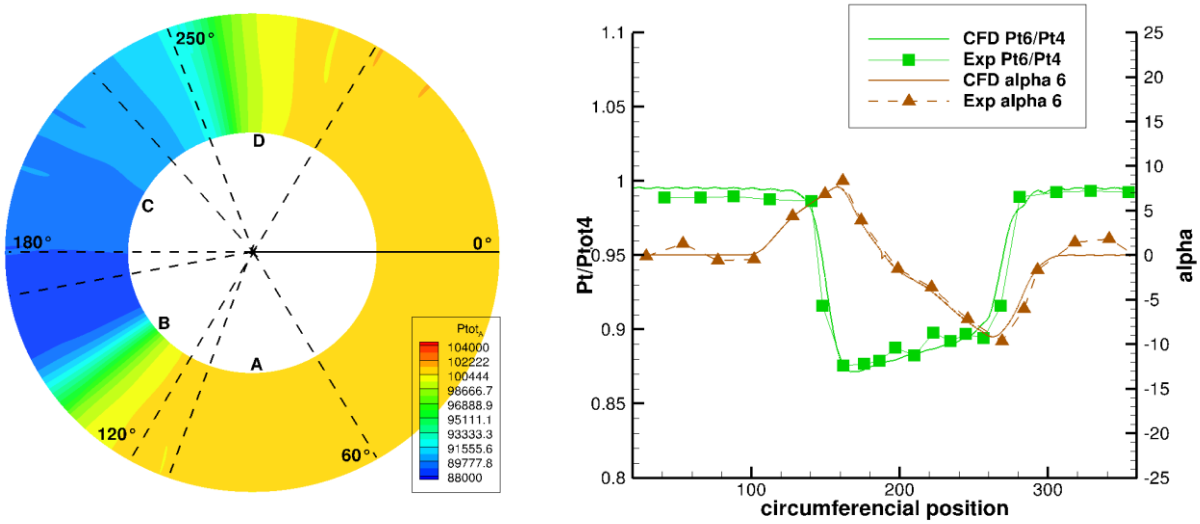

Figure 3: INLET PLANE WITH QUALITATIVE TOTAL PRESSURE DISTRIBUTION AND MEASURED AND PRESCRIBED TOTAL PRESSURE AND INFLOW ANGLE DISTRIBUTION

In Figure 4 the total temperature increase at mid-span is shown for the plane between rotor and stator. The variation of total temperature in the distorted sector is caused by the variation of energy conversion from the rotor to the fluid. Entering the distorted sector the rotor is facing a co-swirl due to the inflow angle variation, initially in the absence of the total pressure variation. This co-swirl leads to a reduction of the blade loading and conversion of energy. As the total pressure distortion becomes more important, it produces an axial velocity drop. With respect to that phenomenon the inflow angle decrease, both the blade loading and the energy conversion are increasing. As a result the total temperature is also increasing. At the end of the distortion sector the blade loading and therefore total temperature as its highest, due to the worst pressure side incidence, is resulting from combined inflow variation and total pressure drop. In general the experimental and numerical results show a qualitative very good agreement. The unique significant difference is at the end of the distorted sector. As already mentioned the blade loading and the total temperature are expected to be highest in this area. As the measured total temperature shows a strong drop at the end of the distorted sector, beyond the undistorted level, it is assumed that the blade loading is too strong in this region and flow separation phenomena occur, which leads to less energy addition. As the simulations were carried out without transition modeling possible separation phenomenon cannot be expected to be predicted correctly by the simulation.

The total pressure rise downstream of the stator is depicted in figure 4 on the right hand side. The periodic total pressure variations of the calculated results are due to the stator wakes. The measurements are not able to resolve the wakes do to the few probe points. With the knowledge of the complexity of the problem, the general trend of numerical and experimental data combines well.

All things considered the simulation of the test case shows good results. The differences are assumed due to modeling reasons, as absence of transition modeling, lack of experimental data, as the shape of the distortion outside of the mid-span region and geometrical uncertainties like tip clearance details. A detailed discussion of the validation was published in [26].

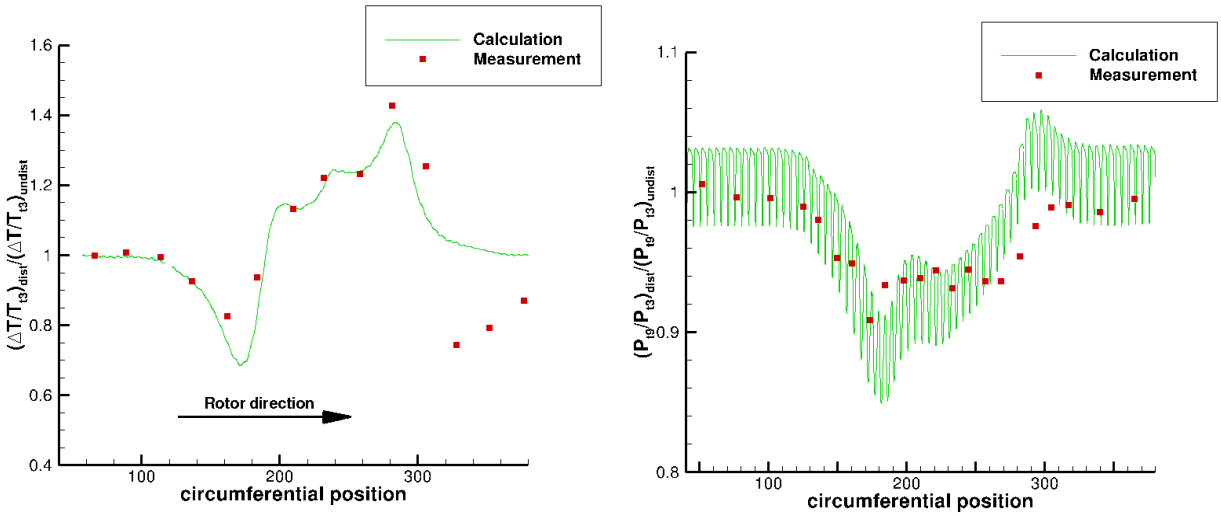

Figure 4: CIRCUMFERENCIAL TOTAL TEMPERATURE INCREASE DISTRIBUTION BETWEEN ROTOR AND STATOR, 50% SPAN AND CIRCUMFERENCIAL TOTAL PRESSURE INCREASE DISTRIBUTION AFTER STATOR

The operating points of the passages are shown in Figure 5. The triangle symbols represent the circumferential averaged operating points related to the experimental averaged total pressure upstream of the wake generating grid and the numerical averaged total pressure downstream of the wake generator, respectively. The total pressure rise difference between them depicts the total pressure loss due to the wake generator. The quadratic symbols represent the operation points of the particular blade passages. The color of the symbols is a coding of the circumferential position. It can easily be seen that a significant number of passages work beyond the stability limit, i.e. the rotor blade leaves the stable working area within the distorted sector and returns back to the stable area after leaving the distorted sector. Therefore the compressor is able to work stable although with a significant part of it working under unstable conditions, as long as the stable part is big enough to damp the distortions and maintain stable behavior. Taking a closer look into the occurring flow phenomena the tip clearance vortex is studied in more detail. The Mach number distribution for various sectors at 98% span is shown in figure 6, the circumferential positions of the sectors A, B, C and D refer to Figure **3**. The rotor is within the undisturbed flow region in sector A and enters the distorted area in sector B. The tip clearance vortex, represented by low Mach number areas, remains its shape in sector A, and is weakened entering sector B. Across sector B the vortex strength increases to getting strongest at the end of sector C and the beginning of sector D. The tip clearance vortex depends on the pressure gradient between suction and pressure side which varies due to different blade loading. The variation of the incidence and blade loading during the rotor is passing the distorted sector leads to the observed variation of the tip clearance vortex. Especially the blockade due to the strong vortex caused by high blade loading in sector C leads to high incidences at the blade tip region and therefore to separation phenomena. A detailed discussion of the occurring flow phenomena can be found in [27].

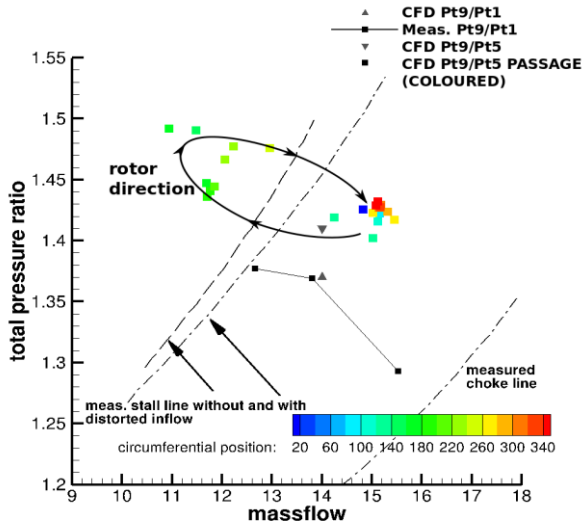

Figure 5: COMPRESSOR MAP WITH PASSAGE OPERATING POINTS, COLORS DUE TO CIRCUMFERENTIAL POSITIONS

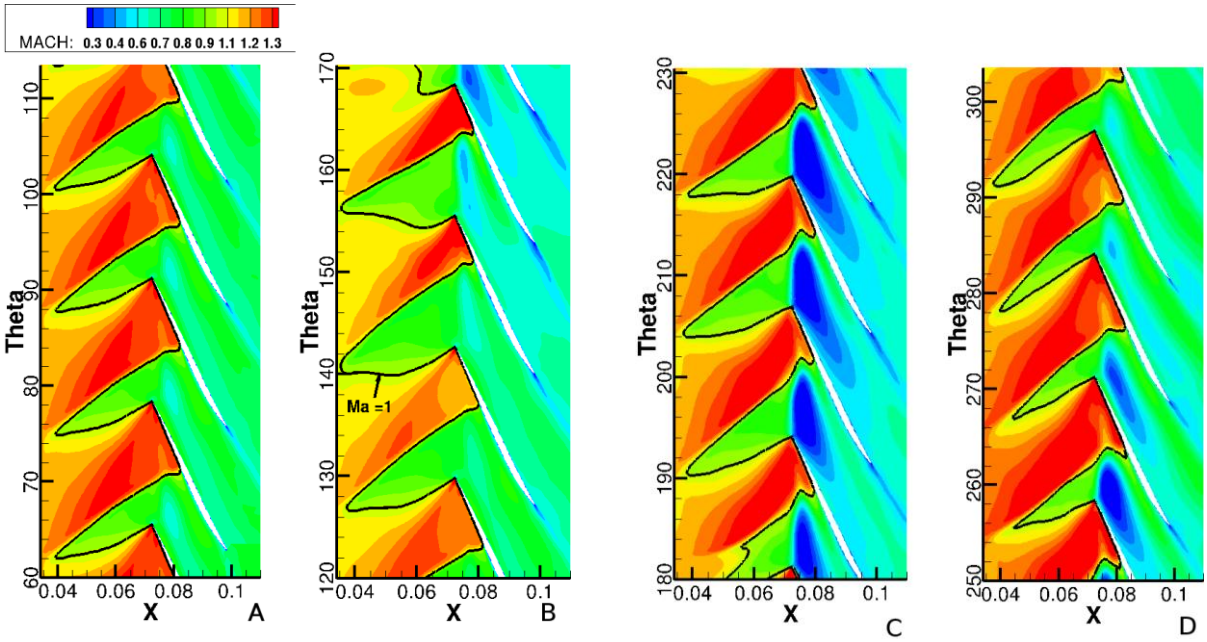

Figure 6: RELATIVE MACH NUMBER DISTRIBUTION AT 98% SPAN, SECTOR A,B,C,D

2. TU Darmstadt Test CASE

After the investigation of the DLR test case the transonic compressor stage of the TU Darmstadt has been examined both numerically and experimentally. The numerical results and comparison of numerical and experimental data will be shown in the following subsection. Before the investigation of the inhomogeneous flow phenomenon the simulation and validation of the compressor stage under investigation with homogeneous inflow is necessary in a first step. In many publications the TUD rotor1/stator1 configuration is simulated with a rotor tip gap of 1.2mm, however, the real rotor tip gap is 1.6mm thus additional simulations were carried out to investigate the influence of the tip gap variation on the compressor performance and the relevant flow phenomena. Extensive studies were also made on the influence of simulation meshes and transition modeling. The measured and numerically predicted

compressor speedlines for 100% rotor speed, two different tip gaps (1.6mm and 1.2mm) and fully turbulent and transition modeling with the multimode transition model by Kožulovic [20] are shown in Figure 7. The use of the transition model is leading to a higher total pressure ratio and to higher efficiency. The qualitative trend of the isotropic efficiency is better predicted with a transition model however the quantitative deviations are higher. The usage of a smaller tip gap leads to a better quantitative prediction of the pressure rise in absence of a transition model, although the calculated characteristic with the original tip shows a better fit of the trend, especially towards lower mass flows and higher pressure rise.

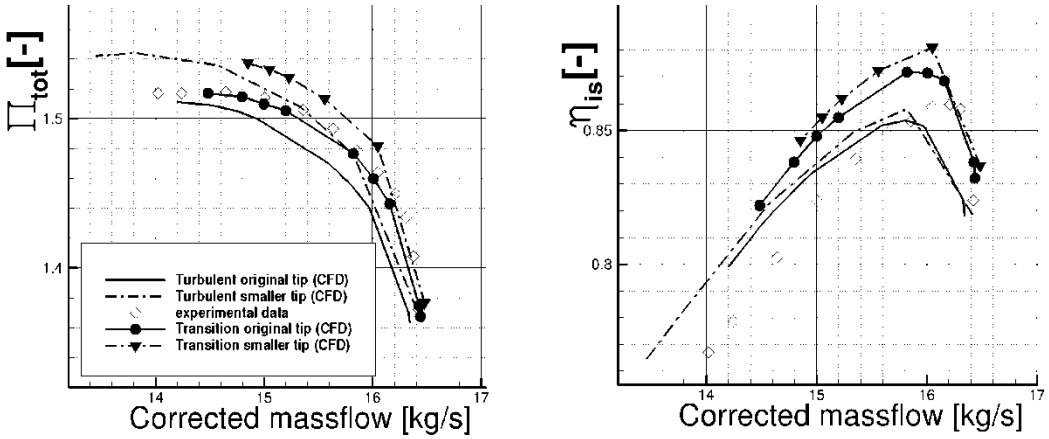

Figure 7: Π_{tot} AND η_{is} FOR THE 100% SPEEDLINE

The predicted and measured results show a very good agreement of global performance parameters. The best result especially for the pressure ratio characteristic shows the combination of original tip gap and transition model. These investigations were published in [28] in detail.

The main shortcoming of the DLR test case is that the inflow distortion was prescribed by an inflow boundary condition. As a result no interaction between distortion source and compressor stage was possible. For this reason the ability to simulate both distortion generator and compressor stage was one design objective of the second test case.

The other objectives were:

- a significant distortion magnitude, if possible a DC60 value higher than 0.2;
- a distortion with radial variation, impinging the rotor at half span
- a periodic unsteady distortion, with stable, but distinct frequency

According to these objectives a distortion generator was designed, in order to generate a local, time periodic total pressure as well as inflow angle variation. A bended square body with rectangular cross-section was chosen which sheds a von Karman like vortex-street of counter rotating pairs of vortices. The distortion generator can be seen in Figure 8. It is fixed by rods and in the background the spinner and the rotor entry plane is shown. The resulting distortions are lateral vortices shedding at the trailing edge of the distortion body. Due to the rectangular cross-section, the Strouhal number and therefore the vortex shedding frequency maintain constant for a wide range of Reynolds numbers. The downstream convecting vortices cause a combined total pressure and inflow angle variation at the rotor leading edge. The frequency and the radial extension of the distortion can be chosen by varying the width B (c.f. Figure 8) of the distortion generator, whereas the circumferential distortion extension is determined by H.

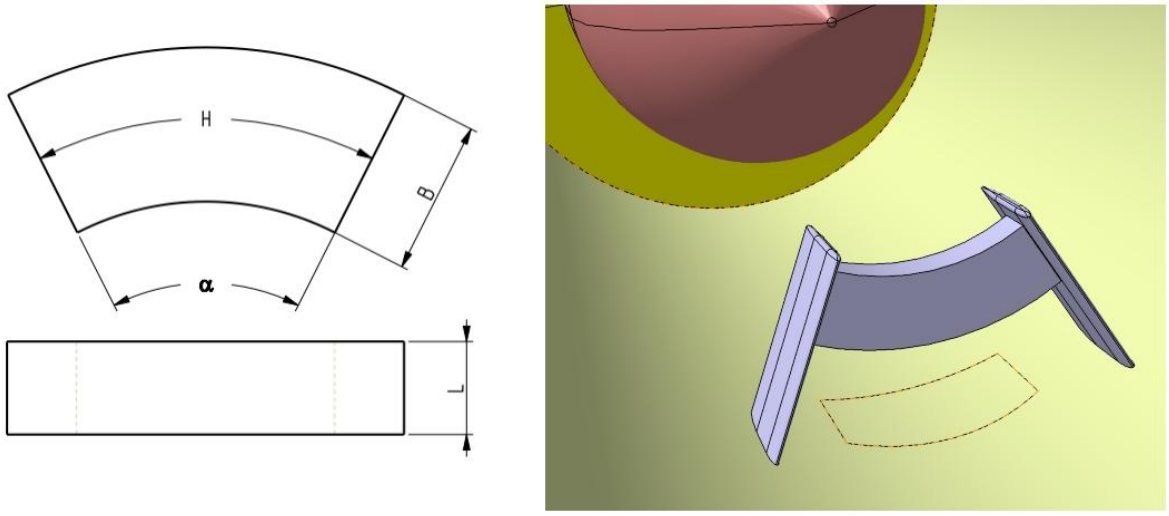

Figure 8: SKETCH OF DISTORTION GENERATOR (LEFT) AND CAD DRAWING OF COMPRESSOR STAGE INLET WITH DISTORTION GENERATOR (RIGHT)

3. Preliminary Results of the TUD Test Case with distorted inflow

The full annulus calculations are extremely time consuming due to their size of the used grids and their unsteady behavior. Given that only preliminary results of the peak efficiency operation point are available so far. Preliminary means in this case that the data is fully converged. However only instantaneous is shown because the output of time series is under process and will take still some more weeks and the data available is not entirely post-processed yet. In Figure 9 the total pressure ratio distribution behind the stator is shown with time averaged experimental and instantaneous numerical data. In the experimental total pressure rise distribution on the left hand side of Figure 9 the 29 vane wakes are well visible. Near the distortion generator position the effect of the distortion cause a decrease of the total pressure rise. Also an effect of strong vane corner separation is evident near hub and tip due to local low pressure rise region which is also reported by [29] for homogenous inflow conditions. The distortion generator has a strong influence and its footprint is clearly visible. Entering the distortion sector the pressure rise is decreasing and after passing the center of the distorted sector the total pressure rise increases beyond the undistorted level to decrease again back to undistorted level.

The pressure rise distribution is in general lower in the numerical data than in the experimental data. That leads to the conclusion that the operation points may differ slightly. However, the behavior of the total pressure rise within the distorted sector is very similar. The total pressure rise begins to decrease in both numerical and experimental data at a position about 5 o'clock position and continue decreasing counterclockwise until three o'clock position to rise again subsequently until the level of the undistorted sector. The total temperature rise distribution is shown in Figure 10 for experimental results on the left and for numerical data on the right side. Again in a counterclockwise proceeding decreases the total temperature rises until about 3 o'clock position and increases in the subsequent. After a maximum at 2 o'clock position the temperature rise decreases again to meet the undistorted level again at 1 o'clock. The experimental data shows a jump at 4 o'clock position which is neither physically expected nor predicted by the numerical simulation. For the sector between 4 and 12 o'clock positions the experimental and numerical data remain qualitative similar but at different levels. The reason for the jump is still unclear and under investigation.

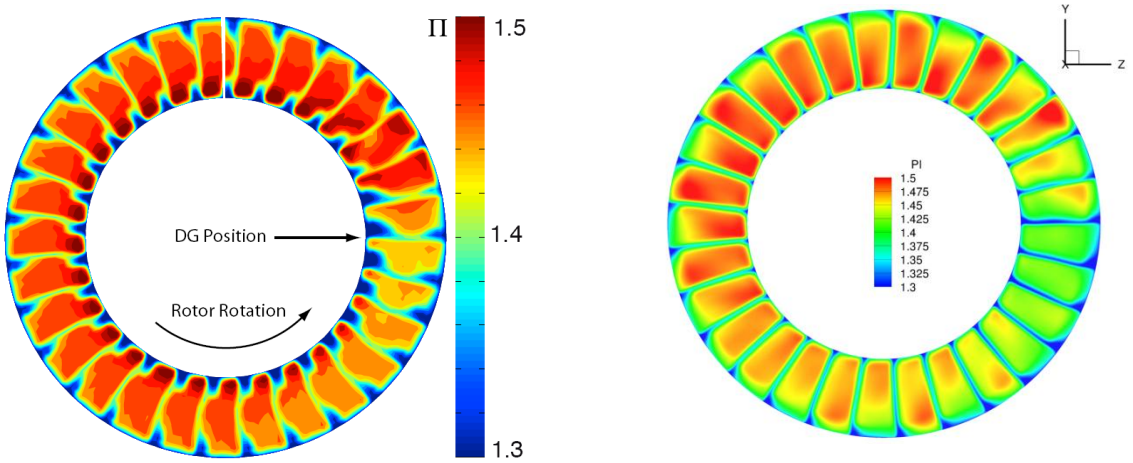

Figure 9: CONTOURPLOT OF TOTAL PRESSURE RATIO DISTRIBUTION DOWNSTREAM OF STATOR AT 100% SHAFT SPEED, PEAK EFFICIENCY OPERATING POINT VIEW UPSTREAM BEHIND STATOR; EXPERIMENTAL DATA [16] (LEFT) AND NUMERICAL DATA (RIGHT)

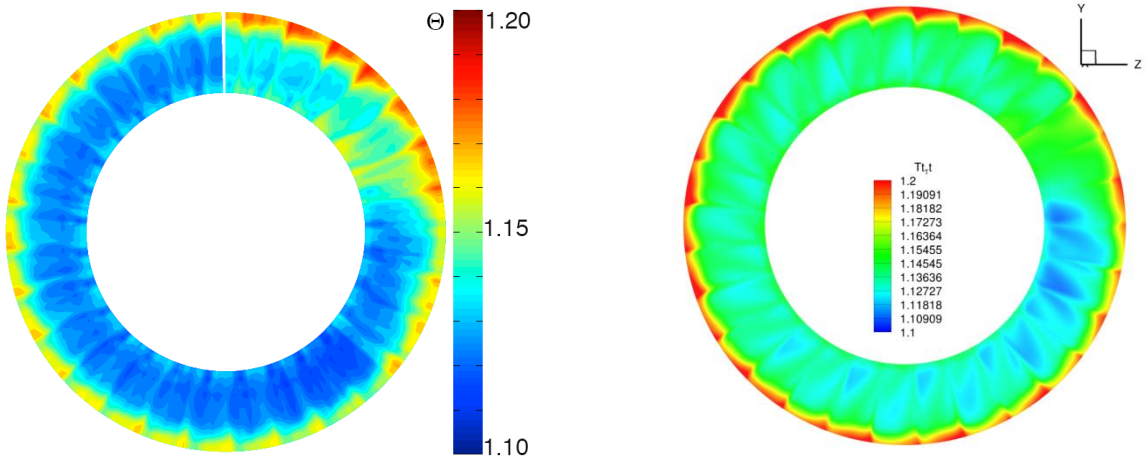

Figure 10: CONTOURPLOT OF TOTAL TEMPERATURE RATIO DISTRIBUTION DOWNSTREAM OF STATOR AT 100% SHAFT SPEED, PEAK EFFICIENCY OPERATING POINT, VIEW UPSTREAM BEHIND STATOR; EXPERIMENTAL DATA [16] (LEFT) AND NUMERICAL DATA (RIGHT)

The local total pressure rise depressions at hub and tip in the experimental total pressure rise distribution are not predicted in the numerical data. Not modeled vane penny slots are supposed to be responsible for the differences. Hence simulations with undistorted inflow conditions were carried out with and without penny slots at the vanes. The resulting total pressure rise distribution is shown in Figure 11. The results without penny slots at the left side of the figure are very similar as the total pressure rise in the undistorted part of the full-annulus calculations in Figure 9. The results with modeled vane slots shown on the right hand side of Figure 11 show a better agreement with experimental data. The corner vortex and as a result of the local total pressure gap are stronger and quite similar to the experimental total pressure distribution in the undistorted part. Altogether the influence on the compressors response due to the distortion is smaller than anticipated with respect to the interaction of the inlet distortion and the compressor.

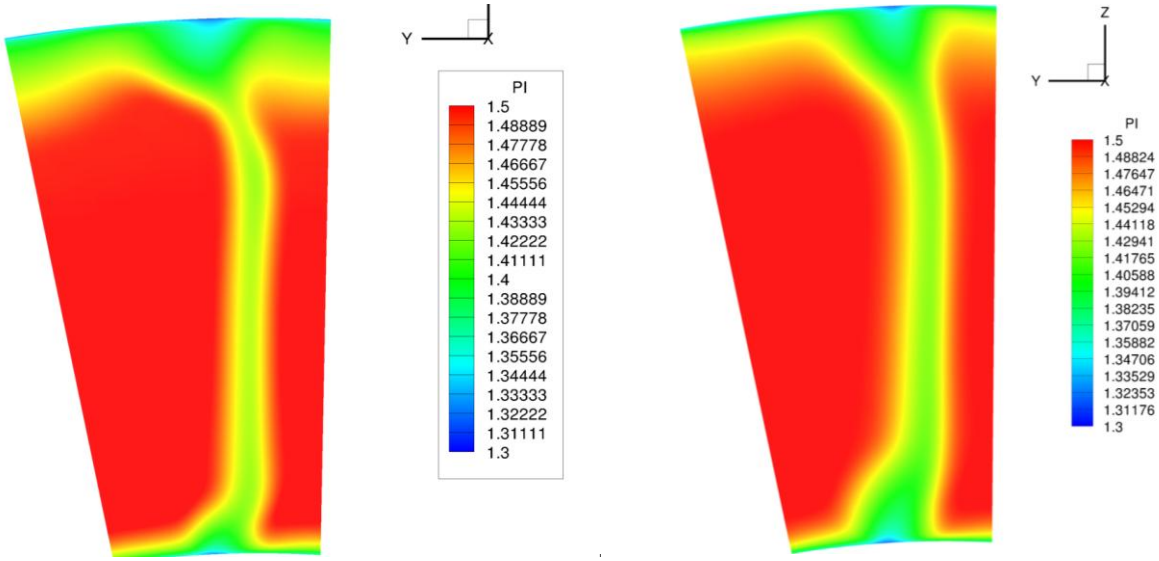

Figure 11: TOTAL PRESSURE RISE DISTRIBUTION FOR HOMOGENOUS INFLOW WITHOUT (LEFT) AND WITH (RIGHT) VANE SEMI-CLEARANCE

IV. CONCLUSION AND OUTLOOK

Numerical investigations of two different transonic compressor test cases tested with different kinds of inlet distortions are presented and discussed in this paper. In a first step a transonic compressor stage has been examined for detailed studies on the influence of inlet distortions on compressor performance which was tested with a steady state total pressure and inflow angle distortion featuring a distribution, which is constant in radial, but variable in circumferential direction. Due to some known shortcomings of the first test case a new test case became available within the frame of the FOR1066 research group. First tests were carried out by TU Darmstadt and further testing is planned for the new phase of the FOR1066 project. Within this research initiative a new distortion generator was designed in order to generate an unsteady, radially and circumferentially varying total pressure and inflow angle distortion. The whole experimental setup including the compressor inlet duct with the distortion generator was meshed and simulated with the flow solver TRACE. Due to the presence of the distortions no periodic flow boundary conditions can be used anymore for the blade passages. Therefore the entire circumference must be meshed and simulated resulting in huge grids (up to 120 million grid elements) and in tremendous computing time even on high performance computers, like the one at the Leibniz Supercomputer center in Munich.
The main conclusion can be summarized as follows. The results of the investigations of the DLR test case show that the used flow solver is able to predict the compressor response due to distorted inflow quite well. It turned out that the correct prediction is more challenging in those sectors where transition and separation phenomena dominate the flow behavior, and transition modeling becomes necessary. Since the DLR test case contains some shortcomings like geometrical uncertainties and only few measurement data are available, the new test case at TU Darmstadt was setup and tested in more detail. First CFD results show a good agreement with the experimental data and are very encouraging. The overall features of the behavior of the distortion and the influence on the compressor performance are captured quite well. Some differences can be explained by shortcoming in modeling details, e.g. the absence of vane penny slots. Further post-processing, validation, and analysis of the numerical data are presently under evaluation. It is also planned to simulate an operating point with higher backpressure near the surge line. In order to create a wide experimental and numerical data base new distortion generators will also be designed and investigated.

Acknowledgments

The members of the FOR 1066 research group gratefully acknowledge the support of the "Deutsche Forschungsgemeinschaft DFG" (German Research Foundation) which funded this research project.

References

[1] C. T. Wakelam, T. P. Hynes, and H. P. Hodson, “Separation Control for Intakes in Crosswinds,” *ISABE-2009-1351*, 2009.

[2] C. T. Wakelam, “Aero Engine Intake Separation Control,” 2009.

[3] P. A. V. Athayde and T. P. Hynes, “Fan-Inlet Flow-Field Coupling,” *ISABE-2007-1141*, 2007.

[4] S. Brix and G. Neuwerth, “The Inlet-Vortex System of Jet Engines Operating near the Ground,” *AIAA Paper No. 2000-3998*, 2000.

[5] A. Hale, A. Hughes, J. Sirbaugh, and D. S. Kidman, “An Investigation Into The Effects Of Highly Transient Flight Maneuvers With Heat And Mass Transfer On The T-38 Air Force Trainer Inlet,” *GT2010-22829*, 2010.

[6] J. Huabing, L. Yajun, Y. Wei, and L. Qiushi, “Experimental Investigation of the Influence of Inlet Distortion in the Stall Inception in a Low Speed Axial Compressor” *GT2009-59139*, 2009.

[7] D. Beale, S. Wieland, J. Reed, and L. Wilhite, “Demonstration of a Transient Total-Pressure Distortion Generator For Simulating Aircraft Inlet Distortion In Turbine Engine Ground Tests,” *GT2007-27222*, 2007.

[8] J. Yao, S. E. Gorrell, and A. R. Wadia, “High-Fidelity Numerical Analysis of Per-Rev-Type Inlet Distortion Transfer in Multistage Fans—Part II: Entire Component Simulation and Investigation,” *Journal of Turbomachinery*, vol. 132, no. 041015, pp. 1-17, 2010.

[9] J. Yao, S. E. Gorrell, and A. R. Wadia, “High-Fidelity Numerical Analysis of Per-Rev-Type Inlet Distortion Transfer in Multistage Fans-Part I: Simulations With Selected Blade Rows,” *Journal of Turbomachinery*, vol. 132, no. 041014, pp. 1-10, 2010.

[10] M. Lecht, “Beitrag zum Verhalten von Axialverdichterstufen,” 1983.

[11] R. J. Dunker and H. Hungenberg, “Transonic axial compressor using laser anemometry and unsteady measurements,” *AIAA Journal*, vol. 18, 1980.

[12] R. Dunker, P. Strinning, and H. Weyer, “Experimental study of the flow field within a transonic axial compressor rotor by laser velocimetry and comparison with through-flow calculations.,” *Journal of Eng. for Power*, 1978.

[13] G. Schulze, “Betriebsverhalten eines transsonischen Axialverdichters,” 1996.

[14] J. Bergner and D. K. Hennecke, “Entwicklung von Verdichterrotoren für einen einstufigen, transsonischen Axialverdichterprüfstand,” *DGLR Jahrestagung* , 2004.

[15] A. Lesser, S. Schulze, R. Niehuis, C. Kähler, and J. Lieser, “Design and Numerical Simulation of an Inlet Distortion Generator,” *14. STAB-Workshop*, 2010.

[16] J. A. Lieser et al., “Compressor Rig Test with Distorted Inflow using Distortion Generators,” *Deutscher Luft- und Raumfahrtkongress, Nr. 241449* , 2011.

[17] P. Roe, “Approximate rieman solvers, parameter vectors and difference schemes.,” *Journal of Computational Physics*, vol. 43, 1982.

[18] D. Wilcox, *Turbulence modeling for CFD*. DCW Industries, Anaheim, 1998.

[19] P. A. Durbin and B. A. Peterson-Reif, *Statistical Theory and Modeling for Turbulent Flows.* John Wiley & Sons, 2014.

[20] D. Kožulović, “Modellierung des Grenzschichtumschlags bei Turbomaschinenströmungen unter Berücksichtigung mehrerer Umschlagsarten.,” 2007.

[21] D. Kožulović, T. Röber, E. Kügeler, and D. Nürnberger, “Modifications of a two-equation turbulence model for turbomachinery fluid flows.,” *Deutscher Luft- und Raumfahrtkongress, Dresden*, 2004.

[22] H. Yang, D. Nürnberger, and H.-P. Kersken, “Toward excellence in turbomachinery computational fluid dynamics: A hybrid structured-unstructured reynolds-averaged navier-stokes solver.,” *Journal of Turbomachinery*, vol. 128, pp. 390–

402, 2006.

[23] H. Yang, D. Nürnberger, and A. Weber, “A conservative zonal approach with applications to unsteady turbomachinery flows.,” *DGLR-JT2002-073*, 2002.

[24] D. Nürnberger, “Implizite Zeitintegration für die Simulation von Turbomaschinenströmungen.,” 2004.

[25] F. Eulitz, “Numerische Simulation und Modellierung der instationären Strömung in Turbomaschinenkomponenten.,” 2000.

[26] A. Lesser, J. Iseler, and R. Niehuis, “Numerical Investigation of a Highly Loaded Axial Compressor Stage with Inlet Distortions,” *GT2011-46457*, 2011.

[27] A. Lesser and R. Niehuis, “Detailed Numerical Investigation of a Transonic Axial Compressor Stage with Inlet Distortions,” *ISAIF10-106*, 2011.

[28] R. Ciorciari, A. Lesser, F. Blaim, and R. Niehuis, “Numerical Investigation of Tip Clearance Effects in an Axial Transonic Compressor.,” *Journal of Thermal Science*, vol. 21, no. 1, 2012.

[29] A. Hergt, R. Meyer, M. W. Müller, and K. Engel, “Loss Reduction in Compressor Cascades by Means of Passive Flow Control,” *GT2008-50357*, 2008.